Crystal structure and magnetism of the Mn_xGa ($1.15 \leq x \leq 2.0$) rare-earth-free permanent magnet system

Rasa Rejali,[1] D. H. Ryan,[1] Z. Altounian,[1] C.B. Boyer,[2] Qingmei Lu,[3] Manli Wang,[3] Hongguo Zhang,[3] and Ming Yue[3]
[1]*Physics Department and Centre for the Physics of Materials, McGill University, 3600 University Street, Montreal, Quebec, H3A 2T8, Canada*
[2]*Canadian Neutron Beam Centre, Chalk River Laboratories, Ontario, K0J 1J0, Canada*
[3]*College of Materials Science and Engineering, Beijing University of Technology, Beijing 100122, China*

(Presented 13 January 2016; received 23 October 2015; accepted 20 November 2015; published online 18 February 2016)

Room temperature neutron powder diffraction has been used to investigate the chemical structure and magnetic ordering of a series of tetragonal (I4/*mmm* #139) Mn_xGa ($1.15 \leq x \leq 2.0$) alloys. Initially ($x < 1.5$) the excess Mn goes on the 2b site with vacancies appearing at the 2a site. For $x > 1.5$ Mn also appears on the 2a site. The manganese atoms on the 4d site carry an almost constant moment of 2.16(6) μ_B/Mn. The loss of magnetisation seen with increasing Mn content is shown to be the result of large (~ 3 μ_B/Mn), antiparallel Mn moments on the 2b, and later 2a sites, and not to a reduction of the Mn moment on the 4d sites. [http://dx.doi.org/10.1063/1.4942557]

I. INTRODUCTION

Manganese-based magnetic compounds are being investigated for two main reasons: (1) they avoid the need for rare earths, (2) they offer a modest-cost/modest performance alternative to the two dominant hard magnet technologies based on $Nd_2Fe_{14}B$ (515 kJ m^{-3}) and $Ba(Sr)Fe_{12}O_{19}$ (45 kJ m^{-3}).[1] Mn frequently carries a large moment, has reasonable chemical stability, and comes at a moderate cost. One possible such system is Mn-Ga. The predicted saturation magnetisation of stoichiometric MnGa is 116 J/T/kg[2] and if a reasonably square loop could be achieved, this would yield an energy product in excess of 200 kJ m^{-3}. Unfortunately, the Mn-Ga binary phase diagram is extremely complex, lacking a single congruently-melting compound. As a result, sample preparation is complex and quality is often poor. The problem has been compounded by focusing on producing technically interesting materials before the intrinsic properties have been understood.

MnGa is expected to adopt the tetragonal P4/*mmm* structure (#123, often denoted as $L1_0$), while Mn_3Ga adopts a closely related tetragonal I4/*mmm* structure (#139, or $D0_{22}$), that is formed by stacking two MnGa cells along the c-axis and redecorating (see Figure 1). In going from P4/*mmm* to I4/*mmm* we pick up an inconvenient selection rule ($l = 2n$) which is made worse by the occupation of the 4*d* site in the I4/*mmm* structure that imposes a further constraint on l: $l = 2n, \forall\ h, k$. The result of these constraints is that it is not possible to distinguish the P4/*mmm* and I4/*mmm* structures on the basis of *any* diffraction data, indeed, the two structures are formally identical: Any packing of a Mn_xGa P4/*mmm* cell can be mapped directly onto an I4/*mmm* cell yielding the same (doubled cell) crystal structure and precisely the same diffraction pattern. For convenience we have used the I4/*mmm* cell here, but identical results can be obtained within the P4/*mmm* cell.

Our interest here is the internal packing of the cell – where does the excess manganese go as we increase x from 1? – and the magnetic ordering of the manganese moments. The poor x-ray contrast between Mn and Ga means that x-ray diffraction cannot be used to study the distribution of Mn within the cell. Indeed, the x-ray diffraction pattern of Mn_xGa is almost indistinguishable from that of a uniform face-centred tetragonal (fct) cell, with the strongest fct-forbidden reflection ((001) for the P4/*mmm* cell) being of order 1% of the intensity of the primary (111) reflection.[4] In

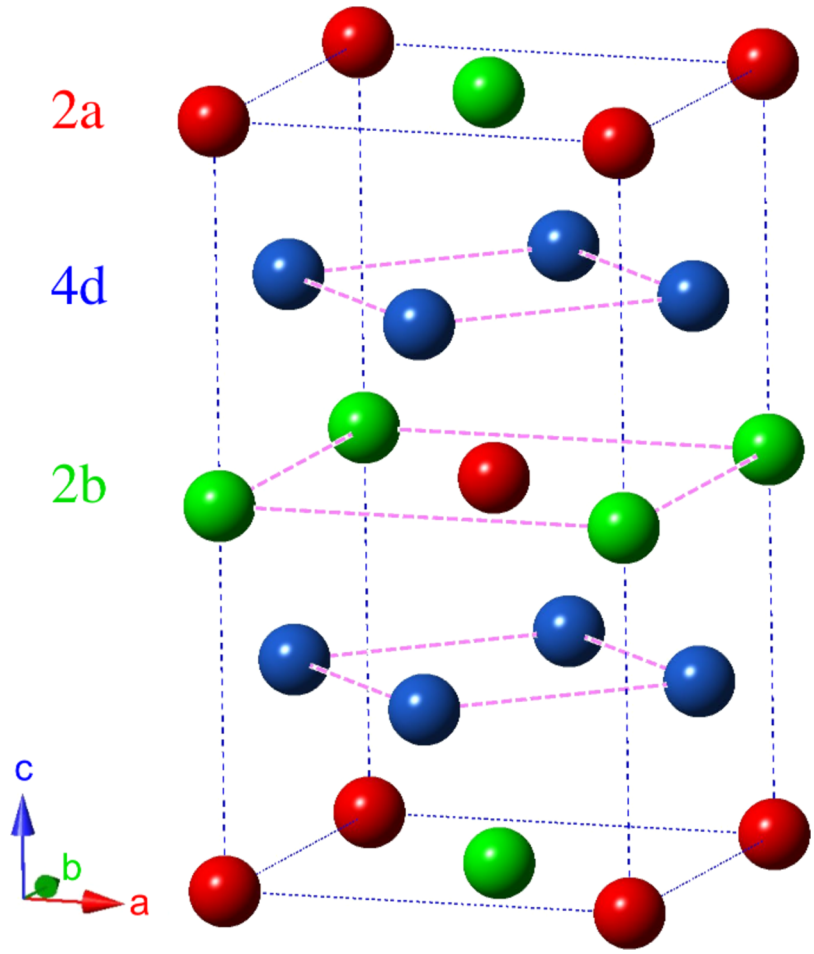

FIG. 1. Tetragonal I4/mmm structure crystal structure adopted by the Mn_xGa system. It can be considered as being constructed from two MnGa (P4/mmm) cells stacked on top of each other, the 2a and 2b sites are equivalent and are occupied by gallium, while the 4d sites are occupied by manganese. In the end member of this series (Mn_3Ga, I4/mmm), the 2a site is occupied by gallium, while both the 2b and 4d sites are occupied by manganese.[3] For the materials studied here, the occupations of the 2a and 2b sites vary (see text for more details).

addition, magnetic order cannot be studied using conventional x-ray diffraction methods. Therefore, we turn to neutron diffraction where there is almost optimal contrast between Mn and Ga (coherent scattering lengths, b_c, are: b_c(Mn) = −3.75 fm and b_c(Ga) = +7.288 fm), and we are also sensitive to the magnetic ordering. This latter sensitivity is important as the magnetisation of Mn_xGa *decreases* with increasing x,[5] suggesting that the additional Mn couples antiferromagnetically (AF) to the ferromagnetic (FM) Mn on the 4d site.

II. EXPERIMENTAL METHODS

A series of tetragonal Mn_xGa (x = 0.15, 0.20, 0.40, 0.80, and 1.00) alloys were prepared by induction melting high purity gallium (99.9%) and manganese (99.5%) in an argon atmosphere. To compensate for evaporation losses during melting, an extra 3 wt.% Mn was added to the alloys. The as-cast ingots were annealed in a tubular vacuum furnace at temperatures, T_a, ranging from 700 K to 900 K for one to seven days and then quenched into ice water. The annealing step is crucial for obtaining single-phase alloys, and the optimal annealing temperature range was found to be quite narrow and depended critically on the composition of the alloy.

Basic structure and phase purity were confirmed using Cu – K_α x-ray diffraction. Magnetic properties were measured using a Quantum Design Physical Properties Measurement System

(PPMS) magnetometer with a maximum magnetic field of 14 T. Neutron powder diffraction experiments were carried out at ambient temperatures on the C2 800-wire powder diffractometer (DUALSPEC) at the NRU reactor, Chalk River Laboratories, Ontario, Canada, using neutron wavelengths (λ) of 1.3272(3) Å and 2.36701(4) Å to cover the widest range of scattering vectors ($0.3\text{Å}^{-1} \leq q \leq 8.0\text{Å}^{-1}$). For every sample, the patterns at each wavelength were counted so as to have at least 20,000 counts in the strongest diffraction peak.

The long and short wavelength diffraction patterns were co-refined to a single structural and magnetic model for each composition using GSAS[6]/EXPGUI.[7] In every case, several models were tried: a mix of Ga and Mn (with and without vacancies) was considered on both the 2a and 2b sites, and the Mn on the 2a and 2b sites was fitted with and without a moment. The 4d site was assumed to be fully occupied by Mn in all samples. In almost all cases, fits of equivalent (and very good) statistical quality could be obtained with a wide range of structural and magnetic models, and so the selection of the best model was further constrained by demanding agreement with the nominal alloy composition and the measured magnetisation. Finally, we sought a consistent model that worked for all compositions studied.

III. RESULTS AND DISCUSSION

A typical set of neutron diffraction patterns for $Mn_{1.8}Ga$ is plotted vs. scatering vector (q) in Figure 2 to show the overlapping scattering ranges covered using the two wavelengths. The ranges were chosen to have several strong peaks in the common region between the long and the short wavelength data so that the patterns could be co-refined with a single set of structural and magnetic parameters. As a first step, all of the datasets were fitted to a LeBail (profile-only) model to establish the instrument profile and lattice parameters. These fits showed that the initial decrease in cell volume was more rapid than would be expected from Vegard's law and then slowed with increasing Mn content (see inset to Figure 4). This suggests that the lower Mn samples may have vacancies in the structure that are filled as more Mn is introduced.

A typical refinement of the 1.3286(2) Å data for $Mn_{1.80}Ga$ is shown in Figure 3. As noted above, fits of identical quality could be obtained with a variety of models, so we sought a model that consistently yielded the correct stoichiometry and observed magnetisation. Figure 4 shows the best results from imposing these constraints and that a consistent model was found. As the upper panel of Figure 4 shows, there is almost perfect tracking between the nominal and fitted compositions:

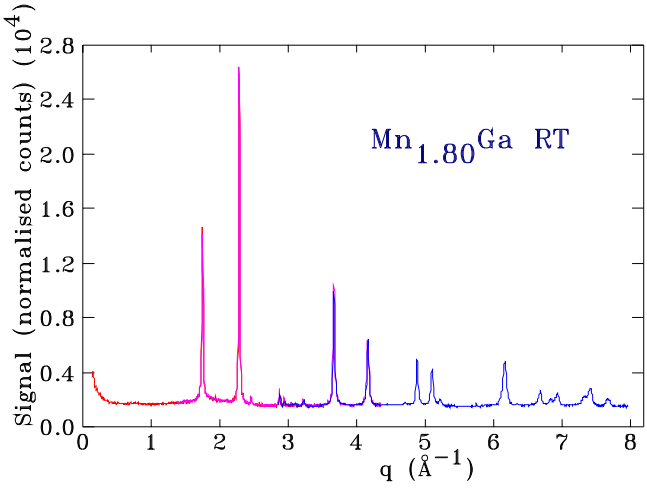

FIG. 2. Neutron diffraction patterns for $Mn_{1.8}Ga$ taken at room temperature using 2.36701(4) Å (red and magneta curves) and 1.3272(3) Å (blue curve) plotted vs. scattering vector (q) to show full range covered. To facilitate comparison, the 1.3272(3) Å data have been scaled down by a factor of 2.8 to adjust for counting time and the higher flux available at this wavelength).

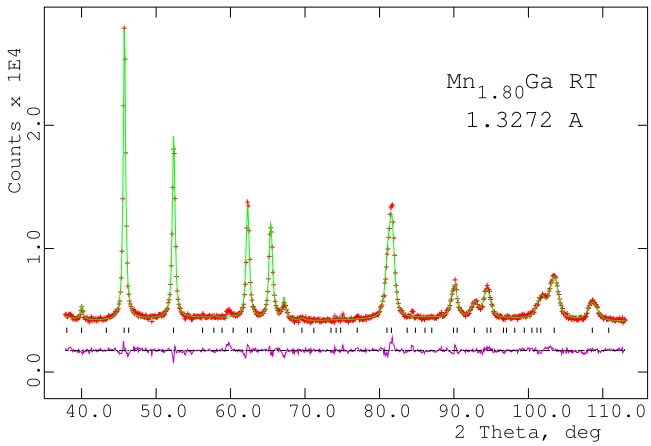

FIG. 3. Fitted neutron diffraction pattern for $Mn_{1.80}Ga$ taken at room temperature using 1.3272(3) Å neutrons. The Bragg markers under the data are for the I4/*mmm* structure. The residuals are plotted under the markers.

The correlation is clearly linear, and the slope of the best fit line is 0.98(4), fully consistent with the expected 1.0.

The model that gave the best fits to the composition starts with the 4d site fully occupied by manganese, opens up vacancies on the 2a site leading to partial occupancy of this site by gallium,

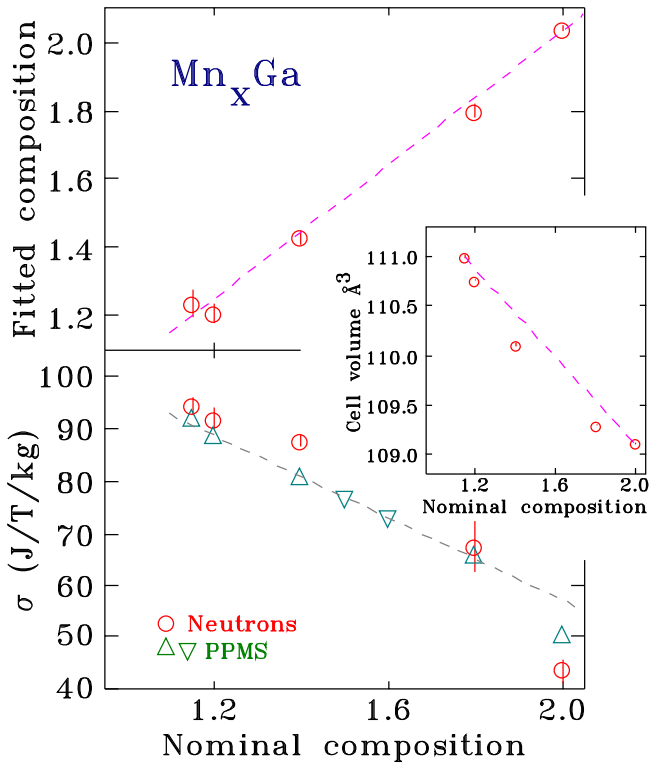

FIG. 4. Stoichiometry (top) and magnetisation (bottom) derived from the neutron diffraction data for the five Mn_xGa samples studied here. The dashed line on the upper panel shows the best-fit with a slope of 0.98(4) confirming that our fits yield the expected stoichiometry. The dashed line in the lower panel shows a linear fit to the magnetisation and emphasises the more rapid drop for $x \geq 1.8$. Correct values for these independently measured parameters were used as consistency checks for the neutron analysis. Magnetisation data for two samples ($x = 1.5$ and $x = 1.6$) are included in the figure but they were not used for the neutron study. The inset shows the unit cell volumes calculated from the fitted lattice parameters.

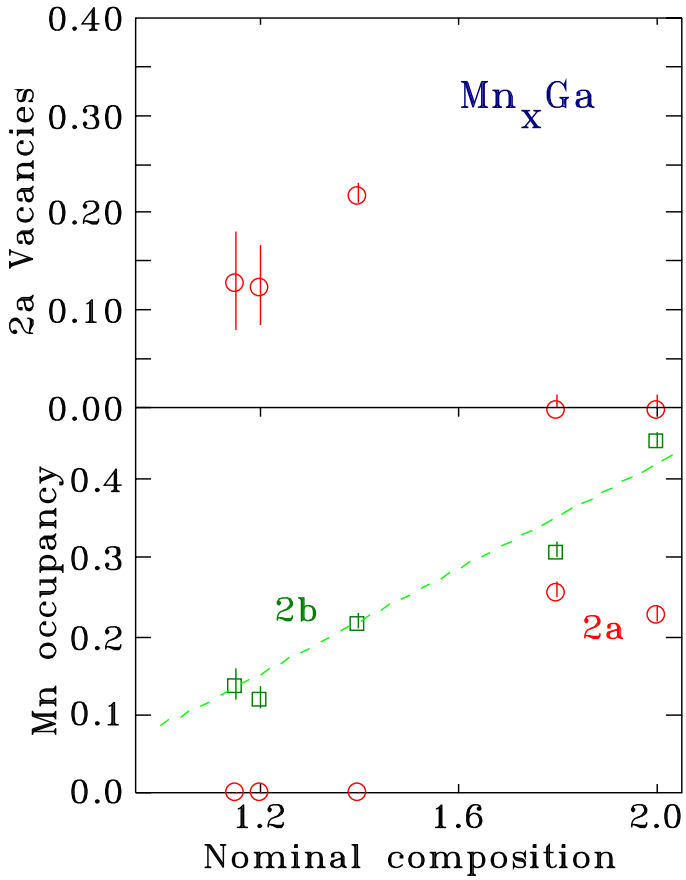

FIG. 5. Top panel: Fractional vacancy rate in the 2a site; Bottom Panel: Mn occupation of the 2a site (as red circles) and 2b site (as green squares) derived from the neutron diffraction data for the five Mn_xGa samples studied here. The dashed line show a best-fit straight line to the Mn occupation of the 2b site. Our analysis suggests that vacancies are present on the 2a site at low x and are filled by Mn atoms for x > 1.5, while Ga on the 2b site is progressively replaced by Mn.

and allows for some manganese to substitute for gallium on the 2b site. This last site (2b) was constrained to be fully occupied by a mix of gallium and manganese atoms. The evolution of the 2a vacancies and the manganese occupation of the 2a and 2b sites are plotted in Figure 5. The 4d site was assumed to be fully occupied by manganese for all of the samples. Many other permutations, such as permitting vacancies on the 2b site or manganese in the 2a site for $x < 1.5$ were tried, but did not yield better agreement with either the magnetisation or the stoichiometry, and ultimately these models were rejected. As the manganese content increases past 1.5, we found that there was a break in the behaviour: The vacancies on the 2a site disappeared, being filled by manganese, and the Mn on this site developed a moment.

Our fits to the magnetism in these materials clearly reveals why the bulk magnetisation drops as more Mn is added. The magnetic structure used as a starting point was based on the I4/mm′m′ magnetic space group that allows for c-axis FM ordering of the Mn moments on the 4d site. This magnetic group also permits c-axis ordering at the 2a and 2b sites. Only collinear magnetic structures were considered here.

As shown in Figure 6, we find an essentially constant moment of 2.16(6) μ_B/Mn for the manganese atoms on the 4d site for all compositions, and a slightly larger (~ 3 μ_B/Mn) moment on the Mn that occupies the 2b site. Various mangetic models were tried for Mn atoms at the 2b sites in the samples with $x < 1.5$. These included: no Mn moment, FM moments and AF moments. When a moment was permitted, even if the initial conditions set it parallel to the Mn(4d) moments, the best fit always had the Mn(2b) moments antiparallel to the Mn(4d) moments. It is this AF ordering between the primary Mn(4d) moments and those on the Mn substituting for gallium at the 2b site

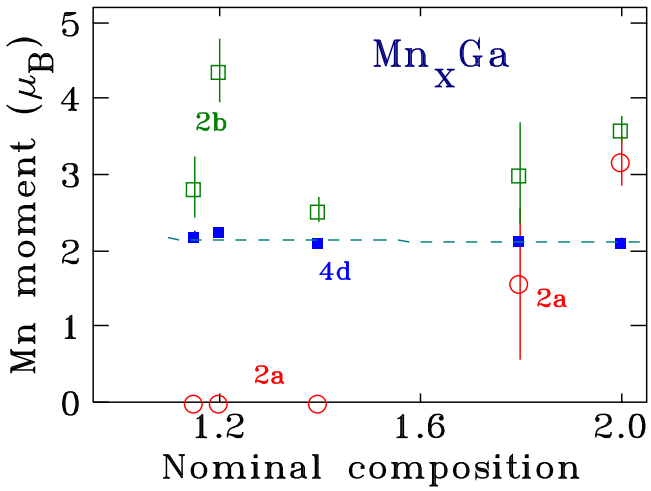

FIG. 6. Fitted Mn moments for the three sites in the I4/*mmm* Mn_xGa structure. The moment of the manganese on the 4d site is essentially constant at 2.16(6) μ_B/Mn (dashed line), while a slightly larger antiparallel moment of ~3 μ_B/Mn appears on Mn atoms that occupy the 2b site (the over-sized moment for the $x = 1.2$ sample is an impurity issue). A similar sized moment is present on the Mn atoms that occupy the 2a site for $x > 1.5$. These are also antiparallel to the Mn moments on the 4d site and so further reduce the net magnetisation.

that leads to the loss of magnetisation with increasing Mn content. The $x = 1.2$ sample had an unidentified impurity and this likely led to the anomalous moment value for Mn on the 2b site in that sample. For $x > 1.5$ the Mn on the 2a site also carries a large (~ 3 μ_B/Mn) moment that is oriented antiparallel to the primary Mn(4d) moments, leading to a further, and more rapid, loss in magnetisation.

IV. CONCLUSIONS

Neutron powder diffraction has been used to determine the site occupancies and magnetic properties of a series of Mn_xGa ($1.15 < x < 2.0$) alloys. We find that fits based on the tetragonal I4/*mmm* structure (#139, or $D0_{22}$) give an excellent description of the data, and that by imposing constraints for nominal composition and magnetisation we are able to develop a consistent model for both the cell packing and magnetic ordering. We find that starting from an (initial) ordered MnGa structure, the excess Mn in Mn_xGa goes on the 2b site with vacancies appearing at the 2a site, and that for $x > 1.5$ Mn also appears on the 2a site. The loss of magnetisation seen with increasing Mn content is shown to be the result of large, antiparallel Mn moments on the 2b, and later 2a sites, and not to a reduction of the Mn moment on the 4d sites.

Some correlations between the cell packing and magnetism were found to be difficult to avoid in the fits and these could be eliminated by obtaining structure-only neutron diffraction data. The samples will be measured at temperatures above their respective magnetic ordering temperatures in the near future and the derived cell packing data will be used to impose a futher constraint on the fits to the magnetically ordered patterns.

ACKNOWLEDGMENTS

Financial support for this work was provided by: the Natural Sciences and Engineering Research Council of Canada, the Fonds Québécois de la Recherche sur la Nature et les Technologies, the State Key Program of National Natural Science Foundation of China (51331003), Beijing Natural Science Foundation (2152006), State Key Lab of Advanced Metals and Materials (2014-ZD07), the Scientific Research Foundation for the Returned Overseas Chinese Scholars, State Education Ministry, and the Fundamental Research Foundation of Beijing University of Technology.

[1] J. M. D. Coey, Journal of Physics: Condensed Matter **26**, 064211 (2014).
[2] A. Sakuma, J. Magn. Magn. Mater. **187**, 105 (1998).
[3] K. Rode, N. Baadji, D. Betto, Y.-C. Lau, H. Kurt, M. Venkatesan, P. Stamenov, S. Sanvito, J. M. D. Coey, E. Fonda, E. Otero, F. Choueikani, P. Ohresser, F. Porcher, and G. André, Phys. Rev. B **87**, 184429 (2013).
[4] T. Mix, K.-H. Müller, L. Schultz, and T. G. Woodcock, J. Magn. Magn. Mater. **391**, 89 (2015).
[5] Q. Lu, M. Yue, H. Zhang, M. Wang, F. Yu, Q. Huang, D. H. Ryan, and Z. Altounian, Scientific Reports **5**, 17086 (2015).
[6] A. C. Larson and R. B. Von Dreele, Los Alamos National Laboratory Report LAUR 86-748 (2000).
[7] B. H. Toby, J. Appl. Cryst. **34**, 210 (2001).